A Flash Flood from a Lake-Enhanced Rainband

DAVID J. NICOSIA AND ERNEST J. OSTUNO

NOAA/National Weather Service, State College, Pennsylvania

NATHANIEL WINSTEAD, GABRIEL KLAVUN, CHARLES PATTERSON, CRAIG GILBERT, GEORGE BRYAN, JOHN H. E. CLARK, AND J. M. FRITSCH

Department of Meteorology, The Pennsylvania State University, University Park, Pennsylvania

(Manuscript received 24 June 1998, in final form 20 October 1998)

ABSTRACT

An analysis of a flash flood caused by a lake-enhanced rainband is presented. The flood took place near Erie, Pennsylvania, on 17 September 1996. It was found that the flood resulted from a complex interplay of several scales of forcing that converged over the Erie region. In particular, the flood occurred during a period when 1) a lake-enhanced convective rainband *pivoted over the city of Erie* with the pivot point remaining quasi-stationary for about 5 h; 2) a deep, surface-based no-shear layer, favorable for the development of strong lake-induced precipitation bands, passed over the eastern portion of Lake Erie; 3) the direction of flow in the no-shear layer shifted from shore parallel to onshore at an angle that maximized frictional convergence; 4) an upper-level shortwave trough contributed to low-level convergence, lifting, and regional destabilization; and 5) a strong land–lake diurnal temperature difference produced a lake-scale disturbance that locally enhanced the low-level convergence.

Analysis of the Weather Surveillance Radar-1988 Doppler radar data from Buffalo, New York, and Cleveland, Ohio, revealed that most of the radar-derived precipitation estimates for the region were overdone *except* for the region affected by the quasi-stationary rainband, which was *underestimated.* Reconstruction of the conditions in the vicinity of the band indicate that cloud bases were considerably lower and equivalent potential temperatures higher than for the areas of precipitation farther east over northwestern Pennsylvania and southwestern New York State. It is postulated that, due to the long distance from the radar sites to the Erie area, the radar was unable to observe large amounts of cloud condensate produced by warm-rain processes below 4 km. Estimates of precipitation rates from a simple cloud model support this interpretation.

1. Introduction

The occurrence of significant weather events as a direct result of forcing from the Great Lakes is well documented (e.g., Petterson and Calabrese 1959; Jiusto 1971; Hill 1971; Lavoie 1972; Lenschow 1973; Hjelmfelt 1990; Byrd et al. 1991; Ballentine et al. 1993; Sousounis and Fritsch 1994). Most of the notoriety of lake-effect events stems from the intense *snow*storms that occur downwind of individual lakes (e.g., over 1.5 m of snow fell near Cleveland, OH, on the eastern shore of Lake Erie, in a 3-day period during November of 1996). These heavy snows typically begin in November and can continue until March. However, as shown by Miner and Fritsch (1997), the potential for similar intense lake-effect events, but manifested as rain instead of snow, occurs as early as August when the water temperature for Lake Erie begins to exceed the air temperature of the adjacent land. Their comparison of the seasonal distribution of precipitation immediately downstream of Lake Erie to that which falls over areas between approximately 100 and 300 km from Lake Erie reveals that large increases in precipitation commence in August and continue through December in the immediate downstream area (Miner and Fritsch 1997). Due to lower static stability and larger contrasts between lake-water temperatures and nearby land temperatures early in the cold season, early season events typically produce heavier precipitation than late season events and often are accompanied by thunder.

On 17 September 1996, a synoptic-scale storm center moved through the mid-Atlantic region and produced heavy rainfall over much of southern New England (Fig. 1a). Concurrently with this broad synoptic-scale event, a smaller but much more damaging heavy rain event occurred over the Erie, Pennsylvania, region (Fig. 1b). More than 177 mm (7 in.) of rain fell over a portion of the lakeside community. The majority of the precipi-

Corresponding author address: David J. Nicosia, National Weather Service Office, 227 West Beaver Ave., Suite 402, State College, PA 16801.
E-mail: nicosia@supercel.met.psu.edu

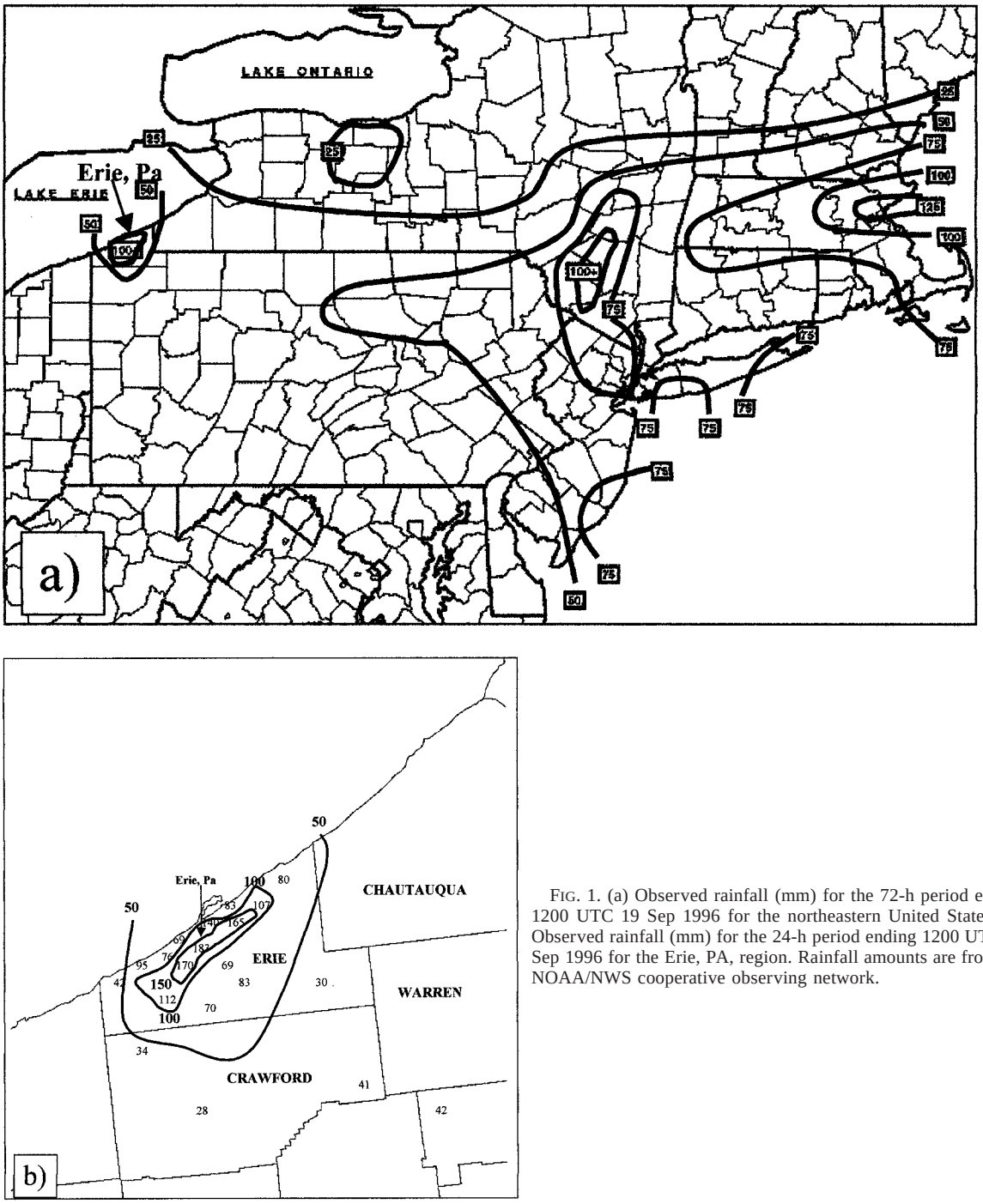

FIG. 1. (a) Observed rainfall (mm) for the 72-h period ending 1200 UTC 19 Sep 1996 for the northeastern United States. (b) Observed rainfall (mm) for the 24-h period ending 1200 UTC 18 Sep 1996 for the Erie, PA, region. Rainfall amounts are from the NOAA/NWS cooperative observing network.

tation fell during a 5-h period from 1500 to 2000 UTC on 17 September with amounts greater than 60 mm (2.5 in.) reported in 1 h. At the height of the event, a rainfall rate of 3 mm (0.1 in.) min^{-1} was recorded by a weather spotter in Mill Creek Township, on the south side of the city of Erie. Flooding was widespread. Several meters of water covered numerous roads, cars floated away, and buildings collapsed. Fortunately, no deaths were reported as individuals in flooded areas were rescued from cars and rooftops. Unfortunately, national forecast guidance failed to anticipate this event. Moreover, the real-time precipitation estimates from the surrounding Weather Surveillance Radar-1988 Doppler (WSR-88D) coverage underrepresented the observed precipitation amounts near the city of Erie.

The purpose of this paper is to document the mete-

orology of the Erie, Pennsylvania, flash flood and to provide information for recognizing and forecasting similar events. Specific objectives include determining whether or not the event was related to lake forcing and elucidating why the radar rainfall estimates were too low. The following section describes the data and methodology used in the analyses. Sections 3 and 4 document the synoptic- and mesoscale conditions, respectively. Section 5 discusses the structure, evolution, and dynamics of a mesoscale rainband that was the feature most directly responsible for the flood. The final section summarizes the results and provides concluding remarks with emphasis on the problem of detection and short-term prediction of similar heavy rainfall events.

2. Data and methodology

The data used in the analyses include the routinely available surface observations and upper-air soundings, WSR-88D radar reflectivities, base velocities and precipitation estimates, visible and infrared Geostationary Operational Environmental Satellite (GOES) imagery, and synoptic-Eta (Black et al. 1993) and 29-km mesoscale-Eta (Black 1994) model output. Radar and satellite loops were employed to help identify and track meso- and synoptic-scale features. Precipitation data was obtained from the National Weather Service (NWS) cooperative observers.

For the mesoscale and synoptic-scale analyses, surface data were subjectively analyzed using 1-hPa and 4-hPa pressure intervals, respectively, following the conventions of Young and Fritsch (1989) and Fritsch and Vislocky (1996). Upper-air data were also analyzed subjectively using standard conventions. Surface streamline analyses were obtained using the analysis system described by Cahir et al. (1981).

In order to isolate and depict mesoscale features, the Barnes (1964) objective analysis technique was employed with the Maddox (1980) scale separation procedure. In this procedure, a bandpass filter is defined in a manner so that the difference between two low-pass filters yields the mesoscale structure. Figure 2 shows the response curves for the two low-pass filters utilized in the analysis; the wavelength band that was passed is also shown. Specifically, in the first filter, the scaling parameters R1 and N1, which are the radius of influence and the gamma factor for the Barnes analysis, were set to 283×10^4 km and 0.03, respectively. These settings removed much of the amplitude of waves smaller than about 300 km while retaining most of the amplitude for meso- and large-scale features. In the second filter, the scaling parameters R2 and N2 were set to 800×10^4 km and 0.40, respectively, so that only large-scale features retained their full amplitude. The difference between the two filters yields a bandpass that isolates features having wavelengths of approximately 500 km, a scale corresponding to the scale of Lake Erie.

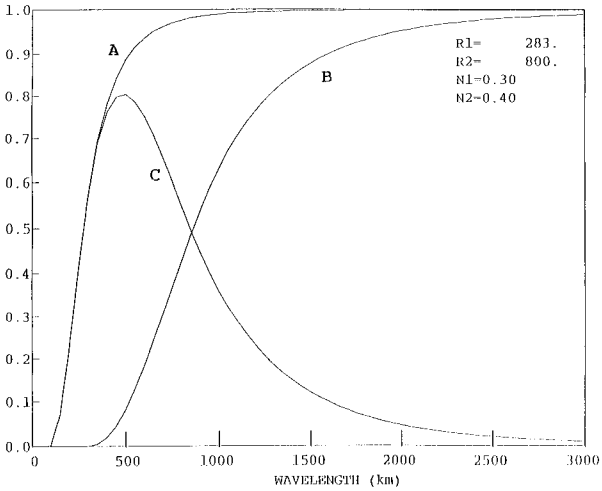

FIG. 2. Distribution of bandpass analysis wavelengths: R1 and N1 are the radius of influence and the gamma factor, respectively, for a Barnes (1964) analysis that includes all but the smallest scale waves (curve A), R2 and N2 emphasize synoptic-scale wavelengths (curve B), and curve C depicts the bandpass (difference between A and B), which highlights mesoscale features.

Estimates of the upper-air conditions over the Erie region during the time of the flooding rains were constructed by using linear time and space interpolation from the surrounding upper-air soundings and then modified at low levels to reflect conditions within and adjacent to lake-induced precipitation bands. The modifications were based on estimates of local temperature and moisture differences between the rainband and its surroundings using the results of Byrd et al. (1991) who took soundings in a similar environment characterized by a single lake-effect band over Lake Ontario. Specifically, Byrd et al. (1991) found that the temperature in a lake-effect band was 3°C greater than the environmental temperature averaged over the lowest 3 km. Soundings were then input into the cloud model of Anthes (1977), from which estimates of parameters such as cloud top, rain rates, vertical motion, etc., were obtained.

3. Synoptic-scale overview

At 0600 UTC 17 September (hereafter 0600/17), about 9 h before the flooding rains began in Erie County, a large and complex extratropical cyclone was moving through the mid-Atlantic region (Fig. 3). The primary low pressure center (over West Virginia) was weakening and a secondary storm center was developing near the Chesapeake Bay. A ribbon of warm moist air was flowing northward up the eastern seaboard and contributing to moderate to heavy rains over eastern Pennsylvania, Maryland, Virginia, and New Jersey.

The normal expectation with this pattern would be for most of the heavy precipitation to remain along the

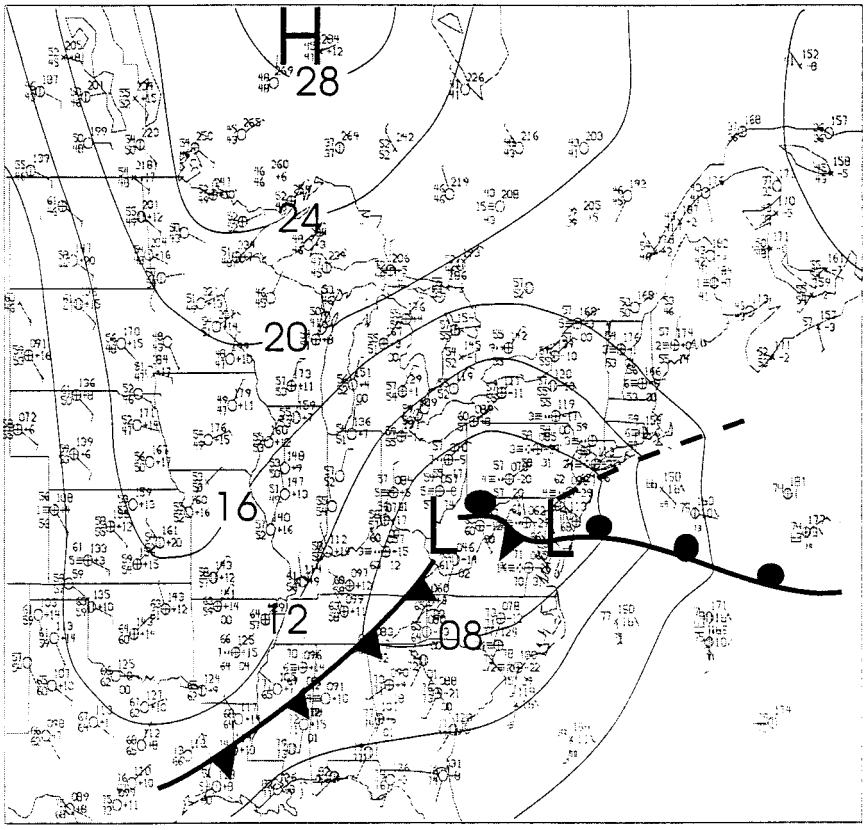

FIG. 3. Surface analysis for 0600 UTC 17 Sep 1996. Contour interval is 4 hPa.

coast in the region of warm advection associated with the developing secondary center and for precipitation west of the Appalachians to decrease as the primary low fills. And, in fact, between 0600 and 1800/17, the widespread heavy rainfall shifted into coastal sections of southern New England and the rainfall over Ohio and western Pennsylvania diminished as cool, polar air flowed south into the mid-Atlantic region. However, complicating this interpretation was a trailing upper-level short wave moving southeastward across the eastern lakes. The Eta Model sea level pressure and 500-hPa height and vorticity analysis for 0000/17 (Figs. 4a,c) show that the primary low pressure center was originally associated with a short wave (labeled SW A) centered over Kentucky. By 1200/17 (Figs. 4b,d), the Kentucky wave had weakened and the trailing short wave (labeled SW B) was emerging as the dominant upper-level disturbance.

By 1215/17, a newly formed, narrow ribbon of clouds stretched southwestward from southern Lake Huron to northwest Ohio, just ahead of the wave-B trough axis (Fig. 5a). As wave B moved eastward across Ohio and western Lake Erie, the ribbon of cloudiness expanded into a large swath of cold cloud tops over eastern Lake Erie, southern Ontario, and northwest Pennsylvania (Fig. 5b). A substantial fraction of the cloud-top temperatures in this region was less than −40°C, signaling that deep convection was under way. Radar data (Fig. 6), taken at approximately the same time as the satellite imagery in Figs. 5a and 5b, indicated that precipitation intensity increased dramatically between 1200 and 1700/17 in a north-to-south axis across northwest Pennsylvania as the wave-B trough axis approached the state.

As the wave-B trough axis continued eastward, it passed through the Erie region shortly after 1800/17 and, by 2115/17, the coldest cloud tops were well to the east, across central New York and northeastern Pennsylvania (Fig. 5c). Likewise, the radar-observed precipitation area associated with the short wave had shifted eastward and decreased in intensity (not shown).

Although the satellite and radar data indicate that deep convective overturning occurred over northwest Pennsylvania, conventional measures of the static stability as observed by the large-scale sounding network infer that there was little potential for deep moist convection in the eastern Great Lakes area. Lifted indices were between +2° and +4°C with K indices ranging from 24° and 29°C in this region. This discrepancy suggests that the environment was locally destabilized by heat and moisture fluxes from the lakes. Local destabilization was favored for several reasons:

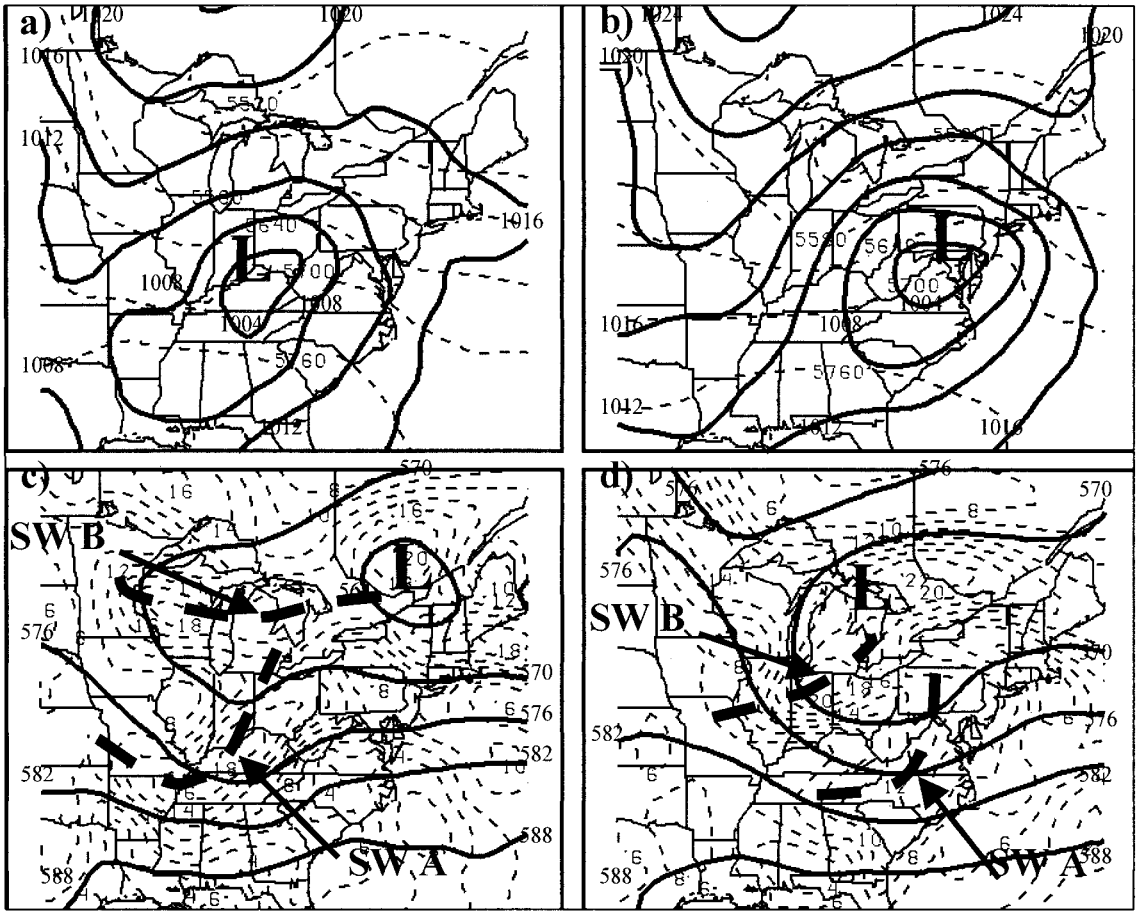

FIG. 4. Synoptic Eta Model 0- and 12-h forecasts of mean sea level pressure (solid, contour interval is 4 hPa) and 1000–500-hPa thickness (dashed, contour interval is 6 dm) valid at (a) 0000 UTC and (b) 1200 UTC 17 Sep 1996. (c) and (d) as in (a) and (b) except for 500-hPa geopotential height (solid, contour interval is 6 dm) and absolute vorticity (dashed, contour interval is 2×10^{-5} s^{-1}).

1) the temperature difference between the surface of Lake Erie and the 850-hPa level exceeded the dry-adiabatic lapse rate,[1]
2) small directional shear[2] prevailed in the surface to 700-hPa layer (Fig. 7),
3) northeasterly flow in the lowest 3–4 km provided airflow over *both* Lake Ontario and Lake Erie (Figs. 3 and 8),
4) the mean flow was parallel to the long axis of both lakes thereby maximizing the fetch, and
5) the arrival of the upper-level cold pool associated with wave B (Figs. 8d,h) occurred over northwest Pennsylvania during this period and intercepted the lake-modified northeasterlies that prevailed over the regions downwind of Lakes Ontario and Erie.

Temperature profiles forecast by the 29-km mesoscale Eta for Erie at 0600 and 1800/17 (Fig. 9a) support the idea that destabilization took place over Lake Erie and northwestern Pennsylvania as a result of a combination of midlevel cooling from the upper-level short wave and lake-forced heating of the lower troposphere. The local nature of this destabilization is evident from Fig. 9b, which compares the 1800 UTC temperature profiles at Erie and Syracuse (New York). The Syracuse profile lacks both the wave-forced cooling at midlevels as well as the overwater low-level trajectories. As a result, the Syracuse sounding is much more stable than the Erie sounding. The destabilization over the Erie region helps to explain why the large mass of convection (Fig. 6b) formed in this area when the short-wave forcing intercepted the lake-modified low-level northeasterly flow.

Although this regional overview provides a general basis for the development of the area of deep convection

[1] Holroyd (1971) showed that virtually all significant lake-effect snowstorms occur when the lake temperature is at least 13°C warmer than the 850-hPa temperature. This indicates that the lapse rate between the lake surface and the 850-hPa level equals or exceeds the dry-adiabatic rate.

[2] Niziol (1987) found that band formation with heavy lake-effect precipitation is enhanced in environments with little directional shear. Strong shear tends to produce a broad stratocumulus layer with little precipitation.

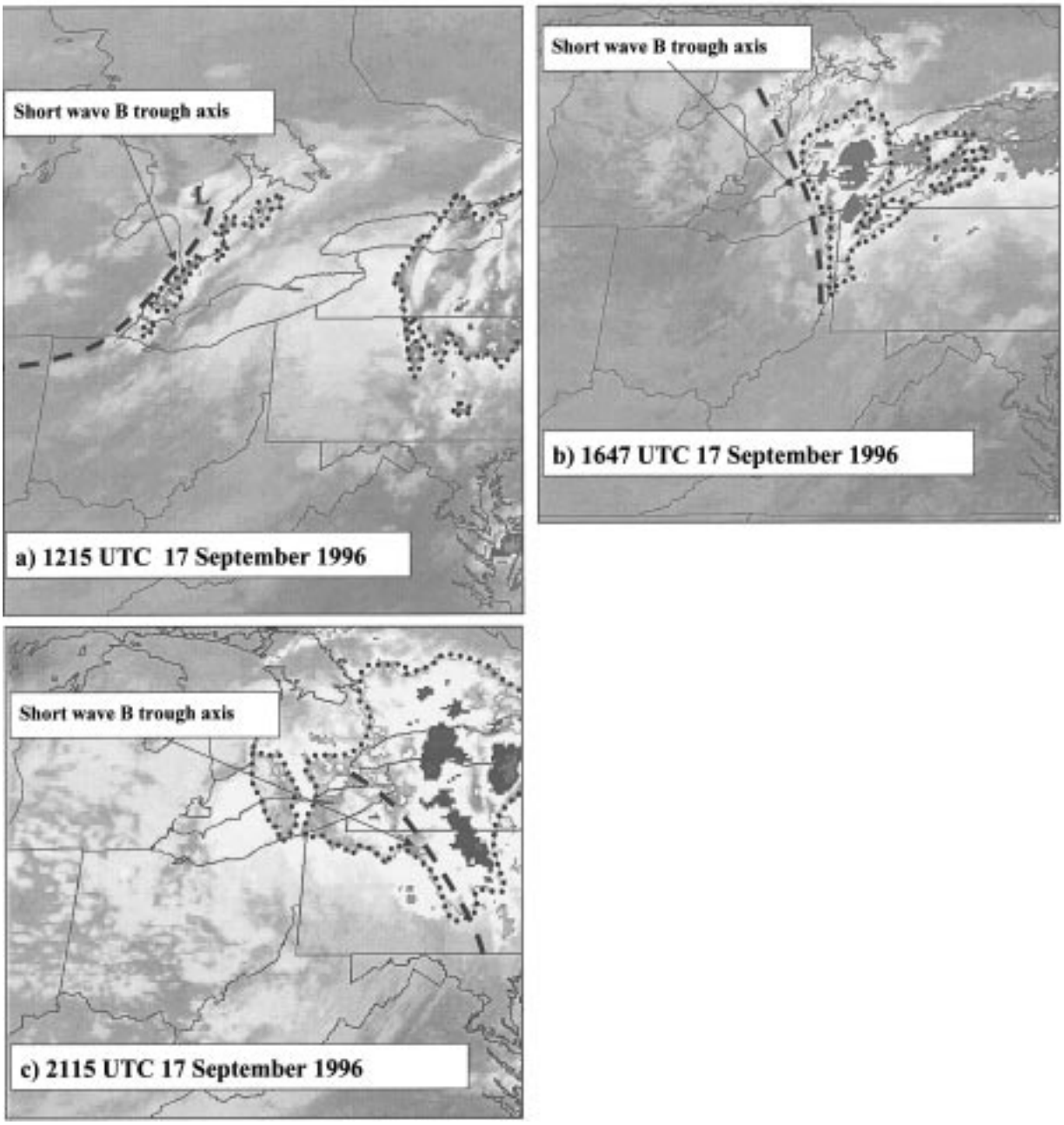

FIG. 5. *GOES-8* enhanced infrared images for (a) 1215, (b) 1647, and (c) 2115 UTC 17 Sep 1996. Blackbody temperature (TBB) < -20°C enclosed by dotted lines. Dark enhancement: TBB < -40°C.

over Lake Erie and northwestern Pennsylvania (Fig. 6b), it does not explain the local maximum in rainfall over portions of the city of Erie. Recall from Fig. 1b that the exceedingly heavy rain fell in a narrow band confined to the southern side of the city. The larger-scale swath of convection only produced rainfall amounts of roughly 25–75 mm (1–3 in.) as evident in Fig. 1. Figure 6b suggests that a mesoscale rainband may have been responsible for the local rainfall maximum. The next section documents the presence of a mesoscale rainband over the city of Erie and presents a detailed examination of the mesoscale events that supported the formation and persistence of this band.

4. Mesoanalysis

As shown in Figs. 3 and 8, cool northeasterly flow dominated the eastern lakes region from the surface to about 700 hPa. However, because Lake Erie temperatures were still relatively high (about 20°C), a pro-

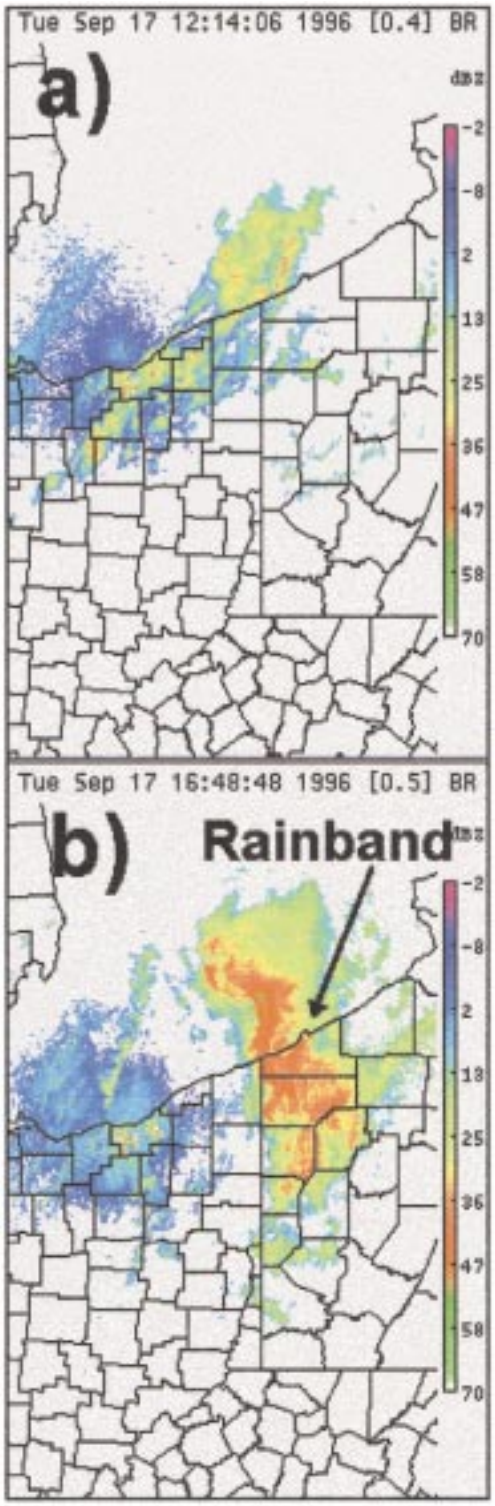

FIG. 6. Cleveland WSR-88D base reflectivity (dBZ) for 0.5° elevation slice at (a) 1214 and (b) 1647 UTC 17 September 1996.

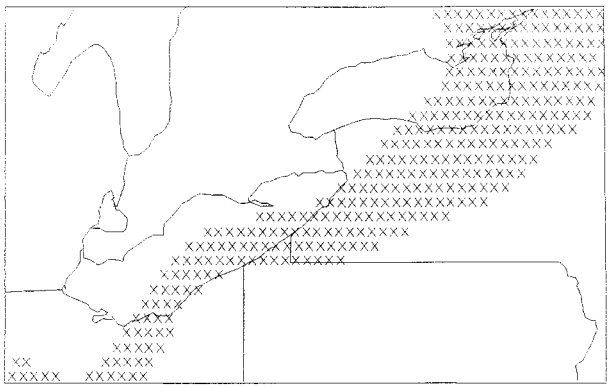

FIG. 7. Area (stippled) with surface–700-hPa directional shear $<20°$ at 1500 UTC 17 Sep 1996.

nounced warm anomaly developed over and slightly downstream of the lake by 1200/17, just prior to the onset of the heavy rains (Fig. 10a). Coincident with the warm anomaly was an elongated mesolow centered near the downstream shoreline that formed overnight (not shown) and persisted through the morning hours (Figs. 10a,b). The mesolow enhanced the pressure gradient on the upstream side of the lake thereby accelerating the flow toward the downstream shore. This condition persisted through the morning and, coupled with the approaching short wave, was instrumental in generating a local maximum in convergence over the downstream shoreline, extreme northwestern Pennsylvania, and southwestern New York. The mesoscale bandpass analysis (Fig. 11), which isolated the lake-scale forcing (Fig. 2), clearly illustrates the local convergence maximum near Lake Erie associated with the lake-induced mesolow analyzed in Fig. 10.

Radar-derived hourly precipitation estimates from the BuffaloWSR-88D show that prior to the arrival of short-wave B (shortly after 1200 UTC), several rainbands arced cyclonically across the Lake Erie region (Fig. 12a). The largest band originated over Lake Ontario and fed into the center of Lake Erie. With the arrival of short wave B during midmorning, this band evolved into an area of intense convection over the northern side of the lake. One of the other rainbands (labeled ''Erie shoreline band'' in Fig. 12a) formed along the northern fringe of the region of maximum surface convergence near the lake-induced mesotrough and within the zone of strongest low-level temperature gradient. Prior to the arrival of wave B, this band was parallel and very close to the Erie County shoreline (Fig. 12a). With the arrival of short wave B, the band intensified and moved inland across the Erie region as it became the dominant mesoscale rainband (Figs. 12b and 13a). Associated with this band was a narrow core of strong inbound velocities (northeasterlies) with speeds up to 22 m s^{-1} (Figs. 13b,d). Notice in Fig. 13b that the shoreline band showed far stronger inbound velocities (northeasterlies) than the two other adjacent bands evident in Fig. 12b.

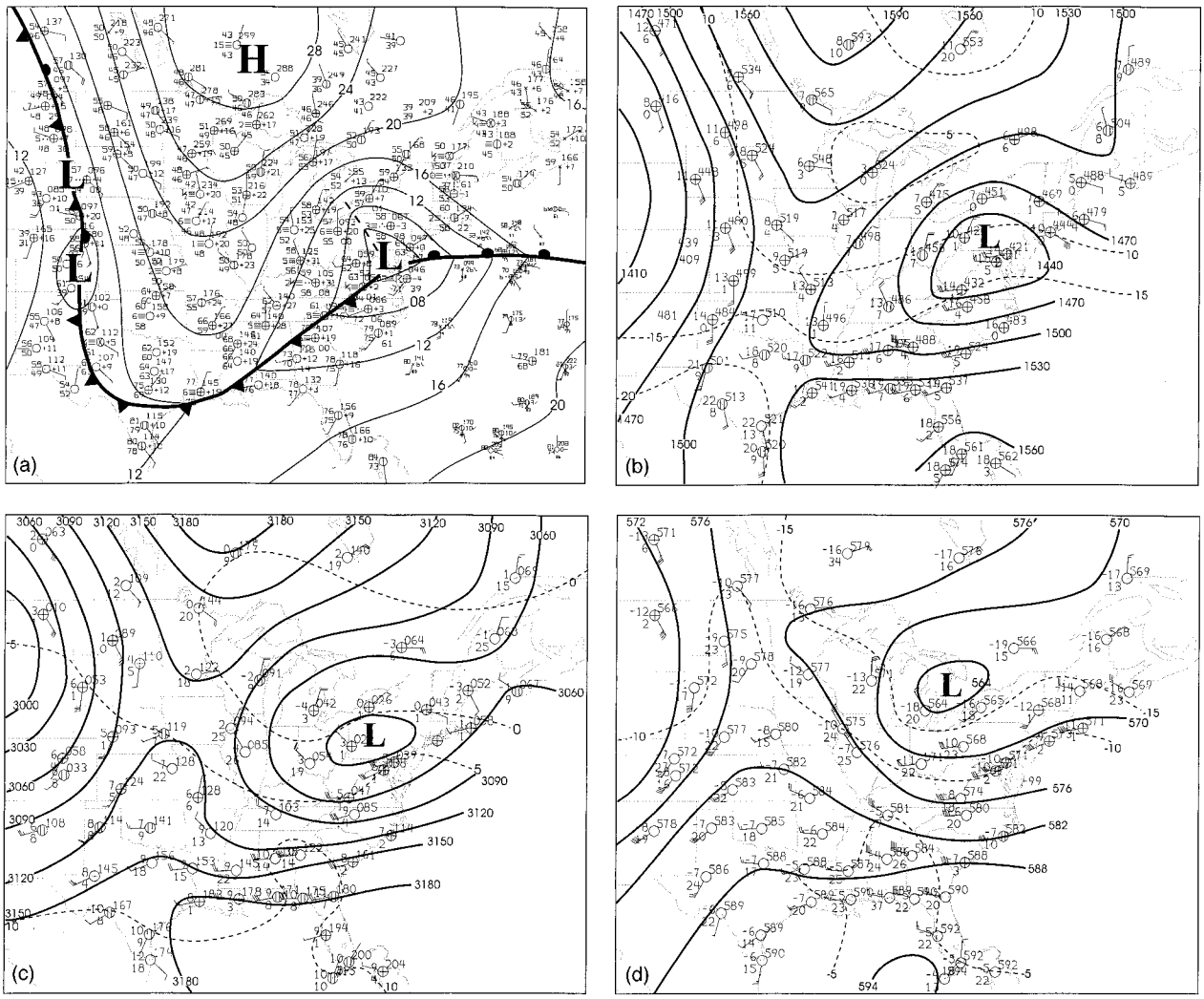

FIG. 8. Surface, 850-, 700-, and 500-hPa analyses for 1200 UTC 17 Sep 1996 (a)–(d) and for 0000 UTC 18 Sep 1996 (e)–(h). All analyses follow standard conventions.

Radar time-lapse imagery of reflectivity and radial velocity indicated that the axis of highest reflectivities in the rainband were closely correlated to the core of the strongest northeasterlies suggesting that the two features were dynamically linked. This core of strong northeasterlies likely was associated with the mesoscale circulation of the rainband. Hence, this narrow core of wind possessed a similar width as the rainband.

Closer examination of the band reveals that the highest reflectivities were parallel to but offset slightly to the southeast of the core of strongest radial velocities (Fig. 13). This arrangement is similar to an event investigated by Weckwerth et al. (1996) in the sense that the core of strongest winds was displaced in the same manner from the highest reflectivities in roll convection observed in Florida. This indicates strong convergence and ascent were prevalent to the left (relative to the direction of flow) of the highest inbound velocities with divergence and descent closer to the core of strong winds. Figure 13d supports this conclusion by showing anomalous inbound velocities (or northeasterly flow) up to 6 km. Since the large-scale flow was westerly at midlevels (see Fig. 8d), it appears that the mesoscale updraft associated with the band transported easterly momentum up from the lower levels, where northeasterly flow was prevalent, into the midlevels. This is supported by the results of Byrd et al. (1991) who showed that lake-effect bands can lift the ambient inversion.

As the short wave moved closer to the Erie region, and also in response to the thermally induced surface trough along the southeastern coast of Lake Erie, the flow in the surface to 700-hPa layer backed (Figs. 14a,b) and the band rotated counterclockwise (Fig. 14c). Low-level winds became progressively more northerly (Fig. 14b) and advected lake-modified high equivalent potential temperature (θ_e) air onshore into the rainband (Fig. 10). Comparison of Figs. 1b and 14c shows that the location of the rainband closely correlates with the

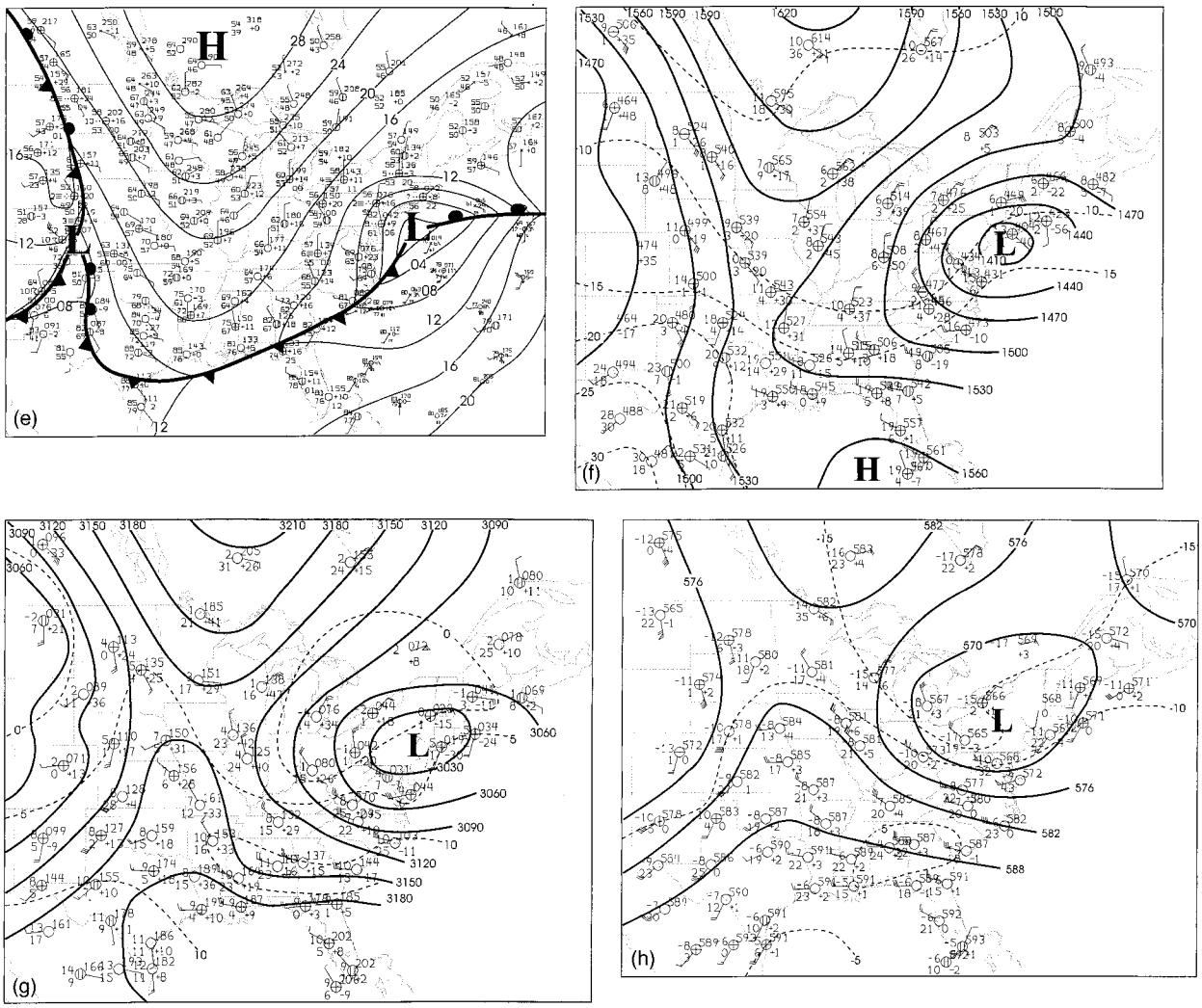

FIG. 8. (*Continued*)

region that received the heavy (>100 mm) rainfall. *Furthermore, the small zone surrounding the quasi-stationary pivot point for the rotating band reported the greatest rainfall amounts.* Surface observations at Erie, Pennsylvania, revealed that cloud bases in the band dropped to approximately 150 m, which, based upon the upper-air analyses and model temperature profiles (Figs. 8 and 9), indicates that warm-rain processes were active in a layer nearly 3 km deep. Moreover, it is evident that the band had a low echo centroid (Caracena et al. 1979) and that a large fraction of the cloud condensate was located in the warm (above freezing) layer undetected by the radar (gray stippling in Fig. 13c).

By early afternoon, the overland temperatures had increased (Fig. 10b) and therefore the lake-induced warm anomaly, mesolow, and associated convergence were weakening. At the same time, the favorable dynamics associated with the upper-level short wave were shifting eastward out of the Erie region (Fig. 8h) signaling the end to the synoptic-scale support for the precipitation. Moreover, the passage of the short wave to the east forced a change in the low-level winds to a more northerly direction inland (Figs. 10b and 14b). The winds also accelerated markedly over the south shore of Lake Erie and onshore at Erie (Figs. 10b and 14b). This change in the low-level winds may have overwhelmed the shoreline parallel convergence zone and ultimately forced the mesoscale rainband away from Lake Erie, its source of heat and moisture. As a result, the shoreline band and larger area of convection dissipated over the region after 1900/17.

5. Discussion—The shoreline rainband

a. Formation of bands

There are several plausible physical mechanisms responsible for the formation of banded precipitation in

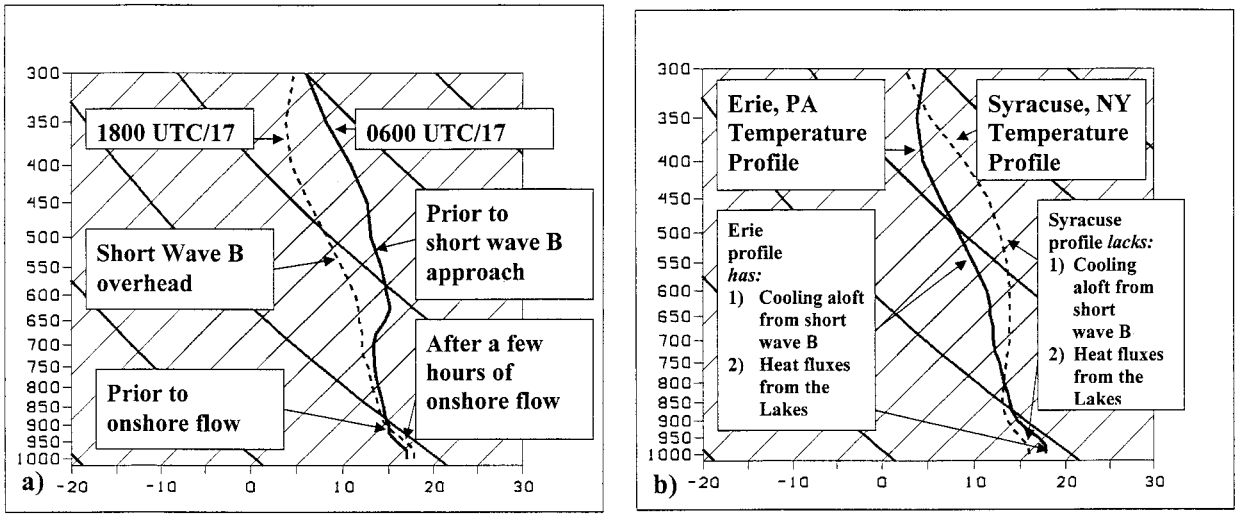

FIG. 9. The 0300 UTC 17 Sep 1996 forecast cycle Meso Eta Model temperature profiles for (a) Erie 3-h forecast valid at 0600 UTC (solid) and 15-h forecast valid at 1800 UTC (dashed) and (b) Erie (solid) and Syracuse, NY, (dashed) 15-h forecast valid at 1800 UTC.

the eastern Great Lakes region *prior* to the arrival of short wave B. One possibility is conditional symmetric instability (CSI). A cross section of mesoscale Eta Model output (not shown) taken perpendicular to the isotherms across northwestern Pennsylvania indicates that CSI was present in the 800–600-hPa layer. Some of the mesoscale rainbands, which formed across northwestern Pennsylvania and southwestern New York, did not tap into the moisture rich environment of the lakes. These inland rainbands may have formed from CSI since the thermal instability was not supportive of convective overturning in these regions. For the band that affected the Erie region, however, a more likely mechanism stems from the modification of the low levels by the warm lake waters. With the addition of heat and moisture to the low levels, the static stability decreased over a broad area downwind of Lake Ontario (across western New York, a part of northwestern Pennsylvania, and along the long axis of Lake Erie). It is postulated that the precipitation bands formed from a thermal instability in the presence of unidirectional speed shear favoring a roll-like circulation. Additionally, strong convergence was present over Lake Erie in association with a lake-induced surface pressure trough that was aligned along the long axis of Lake Erie (Fig. 10).

The focus of this section, the rainband that was most directly responsible for the Erie flood, is evident in the radar reflectivity and radial velocities (Figs. 13a,b). A narrow core of strong inbound velocities (northeasterlies) lies in close association with the high reflectivities of the mesoscale rainband. The correlation between the narrow core of strong northeasterly winds and the highest

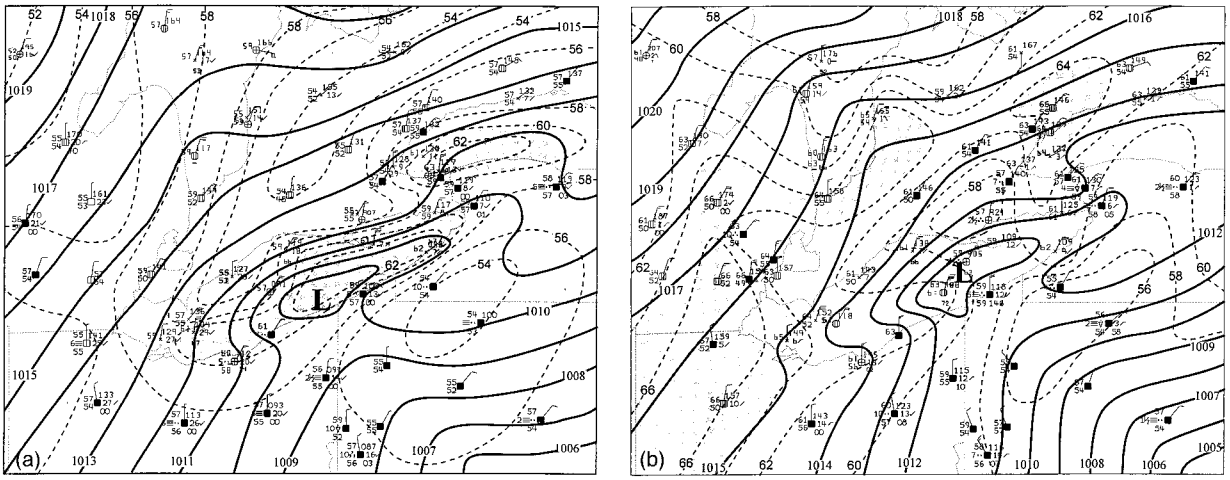

FIG. 10. Surface mesoanalyses of temperature (dashed lines, contour interval is 2°F) and pressure (solid lines, contour interval is 1 hPa) for (a) 1200 and (b) 1800 UTC 17 Sep 1996. Temperatures warmer than 60°F in (a) and 64°F in (b) are shaded.

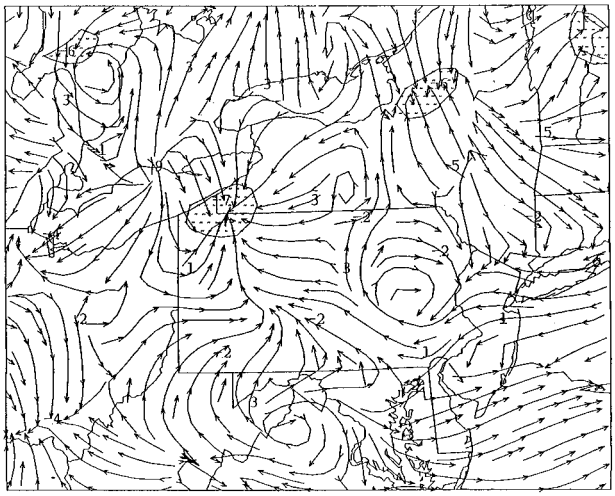

FIG. 11. Streamline analysis of the bandpass-derived mesoscale mean winds for the period 1600–1900 UTC 17 Sep 1996. Shaded regions denote areas of convergence $> 5 \times 10^{-5}$ s^{-1}.

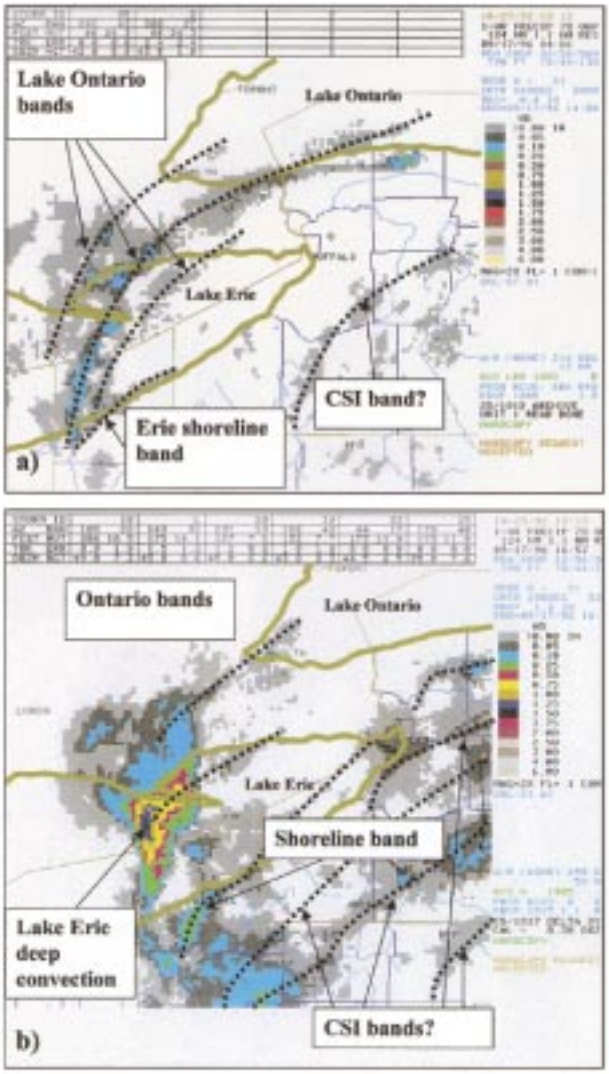

FIG. 12. Buffalo, NY, WSR-88D precipitation estimates for 1-h periods ending at (a) 1401 and (b) 1657 UTC 17 September 1996.

reflectivities suggests that the enhanced northeasterlies were a part of the circulation that supported strong ascent within the rainband. The strong northeasterly flow in Fig. 13b is consistent with simple thermal wind arguments assuming the flow parallel to the rainband is close to geostrophic balance. The ageostrophic response (perpendicular to the band) of the wind to a drop in pressure associated with a warm anomaly over southern Lake Erie is to force the winds to back or become more northerly over the central and northern portion of the lake. This clearly is evident in the surface mesoanalyses (Fig. 10) during the height of the warm anomaly over the lake. Conversely, over the land southeast of the band, the ageostrophic response of the wind field would be to veer (become more easterly) and flow more toward the band. Wind speeds over the land were far less than the winds over the lake water suggesting that the majority of the convergence arose from air parcels converging into the band from across the lake. Since it is assumed that the flow along the rainband is nearly geostrophic, the parcels crossing the lake in the low levels are turned to the right from the Coriolis force leading to enhanced northeasterly flow along the band. The component of the ageostrophic winds from the land appeared to be negligible, which would tend to decelerate winds along the band. This result is consistent with the fact that the air over the lake has less frictional drag.

Regardless of the mechanism of its formation, the mesoscale rainband that persisted over Erie *intensified* with the approach of the upper-level short wave. This agrees with the notion that the wave-forced vertical motion deepened the vertical extent of the roll circulation evident in the radar data by raising the inversion height (Fig. 9a) and allowing the convection to grow vertically. Figure 13d, which shows a radial velocity cross section, indicates that the northeasterly flow grew to 6 km in depth as wave B passed by. This is much higher than the depth of the ambient northeasterly flow as inferred from the upper-air analyses (Fig. 8). As the short wave moved closer to western Pennsylvania, the band rotated counterclockwise and worked inland into Erie County. The shift in orientation was a result of the winds in the lowest few kilometers backing to a more northerly direction as the short wave approached. The result of the band's rotation was that it *pivoted* near the city of Erie upon moving inland. Therefore, it remained nearly stationary over the southwest part of the city of Erie and, thereby, generated the flooding rains (cf. Fig. 14c and 1b).

b. Role of friction

Changes in friction as a result of the land–lake interface may also have played a role in the intensification

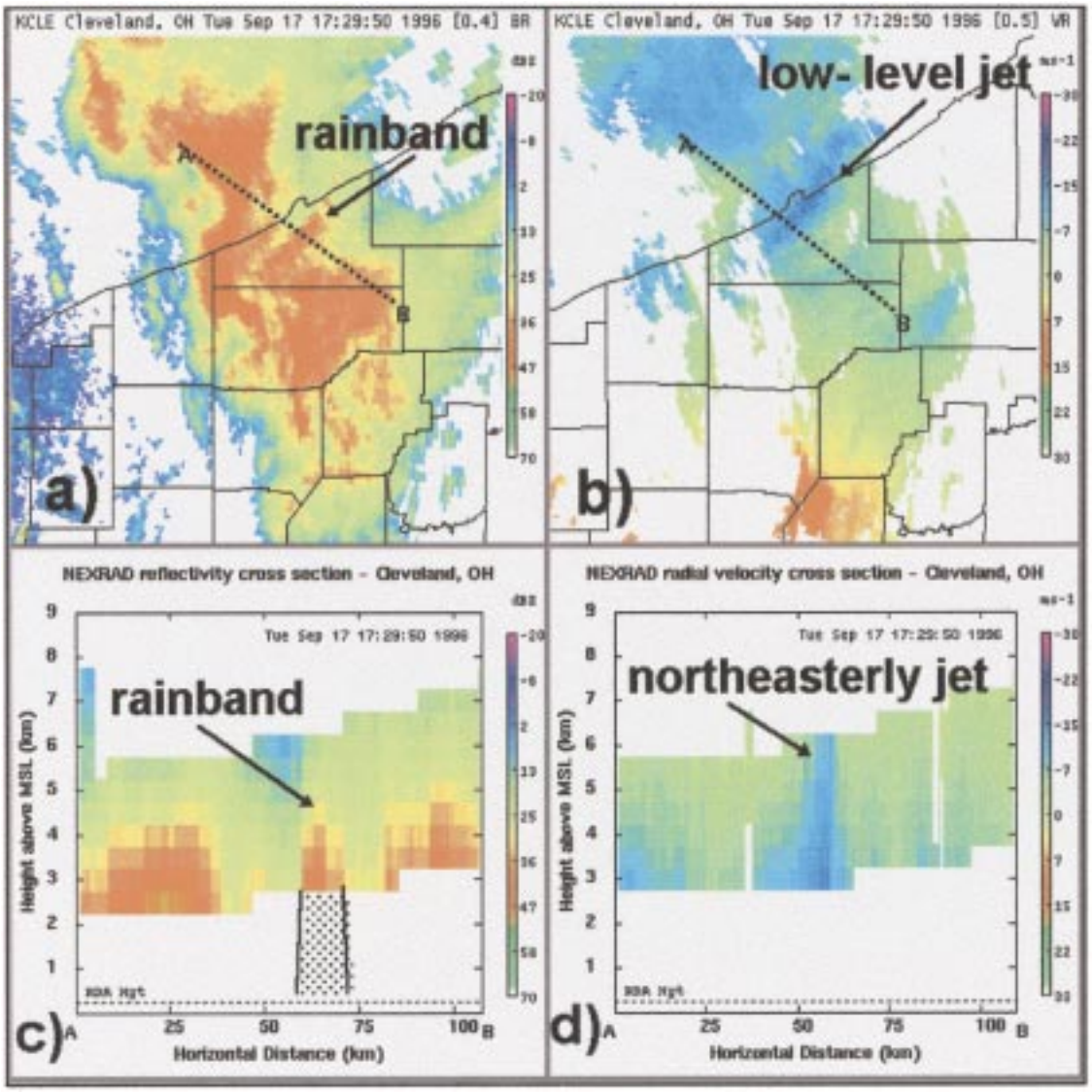

FIG. 13. (a) Cleveland WSR-88D base reflectivity (dBZ) 0.5° elevation slice at 1729 UTC 17 Sep 1996, (b) same as (a) except for base velocity (m s^{-1}), (c) base reflectivity (dBZ) cross section from point A to B in (a), and (d) same as (c) except for base velocity (m s^{-1}). Gray stippling in (c) denotes portion of convection undetectable by the Cleveland radar due to the ascension of the radar beam with distance.

of the narrow rainband. Frictional effects associated with a land–water boundary are influenced by two factors.[3]

1) Due to less frictional drag, the wind is closer to being in geostrophic balance (smaller ''crossing'' angle) over water than over land. This change in crossing angle between the wind and isobars from the water to the land leads to divergence or convergence over the land depending upon the pressure gradient and direction of the flow. This effect is maximized when the flow is parallel to the shoreline.
2) Increased frictional drag over the land, when compared to over the water, leads to a greater wind speed over water when compared to that over land. Thus, depending on the direction of the flow, convergence or divergence occurs in the vicinity of the shoreline. This effect is maximized when the flow is perpendicular to the shoreline.

Early in the day, the surface winds were roughly parallel to the Lake Erie shoreline from the east-northeast. With a large anticyclone situated over Canada and a surface low well to the southeast, the pressure gradient

[3] A theoretical and mathematical basis for these two effects is presented in the appendix.

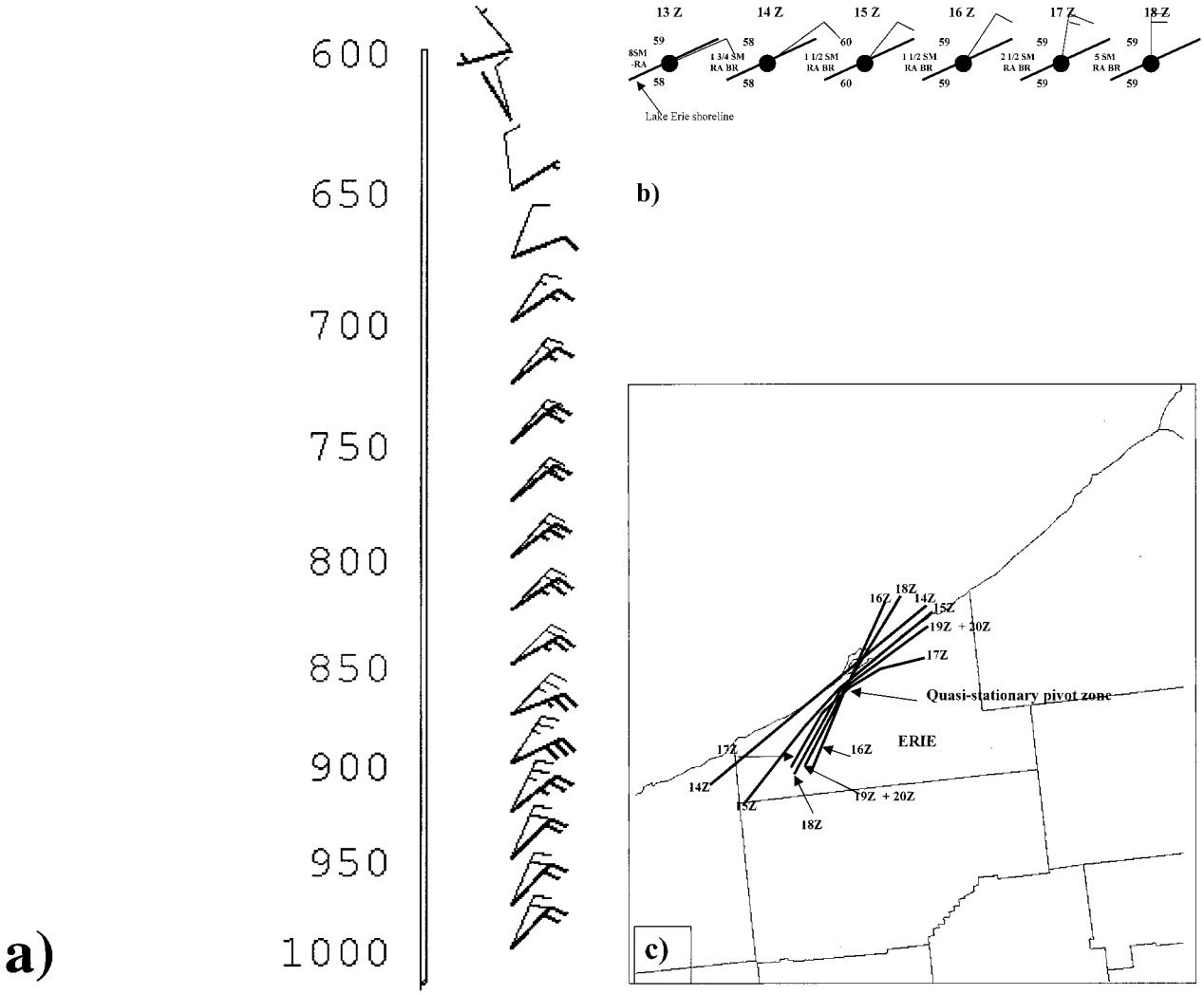

FIG. 14. (a) Meso Eta Model winds (full barb = 5 m s^{-1}) from 1000 to 600 hPa at 1200 (dark) and 1800 UTC (light) 17 Sep 1996. (b) Erie hourly station plots for 1300–1800 UTC, (c) axis of the rainband at 1-h intervals (locations inferred from the Cleveland WSR-88D 0.5° elevation scan base reflectivity from 1400 to 2000 UTC).

force would favor a more easterly wind over the lake and a more northeasterly flow over the land due to a larger crossing angle between the wind and isobars over the land. Thus, initially with shoreline parallel flow from the northeast, frictionally forced low-level divergence would occur over the land in Erie County. As the regional flow backed during the morning hours, the frictional effect associated with different crossing angles between the land and the water diminished. Conversely, the frictional effect associated with different frictional drag between land and water increased as a more onshore flow developed in time. As shown in the appendix, the point at which speed convergence from onshore flow overtook the divergence from the different crossing angle is related to the angle that the surface isobars make with the shoreline. For a nearshore average crossing angle of 30° between the surface wind and isobars, the transition from divergence to convergence occurs when the surface isobars make an angle of approximately 35° with the shoreline.

The Erie rainband underwent a rapid amplification between 1500 and 1600 UTC. According to Fig. 14, the rainband slowly rotated counterclockwise about its pivot point between 1400 and 1800 UTC. The rotation was not steady as witnessed by the anomalous orientation it took at 1700 UTC. At the same time, according to Figs. 8a and 8e, the surface isobars also rotated counterclockwise. They achieved the critical angle of 35° for the onset of convergence approximately when the rainband amplified. Thus, we have a plausible explanation for the amplification. Since the rainband was associated with a core of strong winds in the lowest levels, this convergence effect was maximized within the flow associated with the rainband. In addition, this increasingly con-

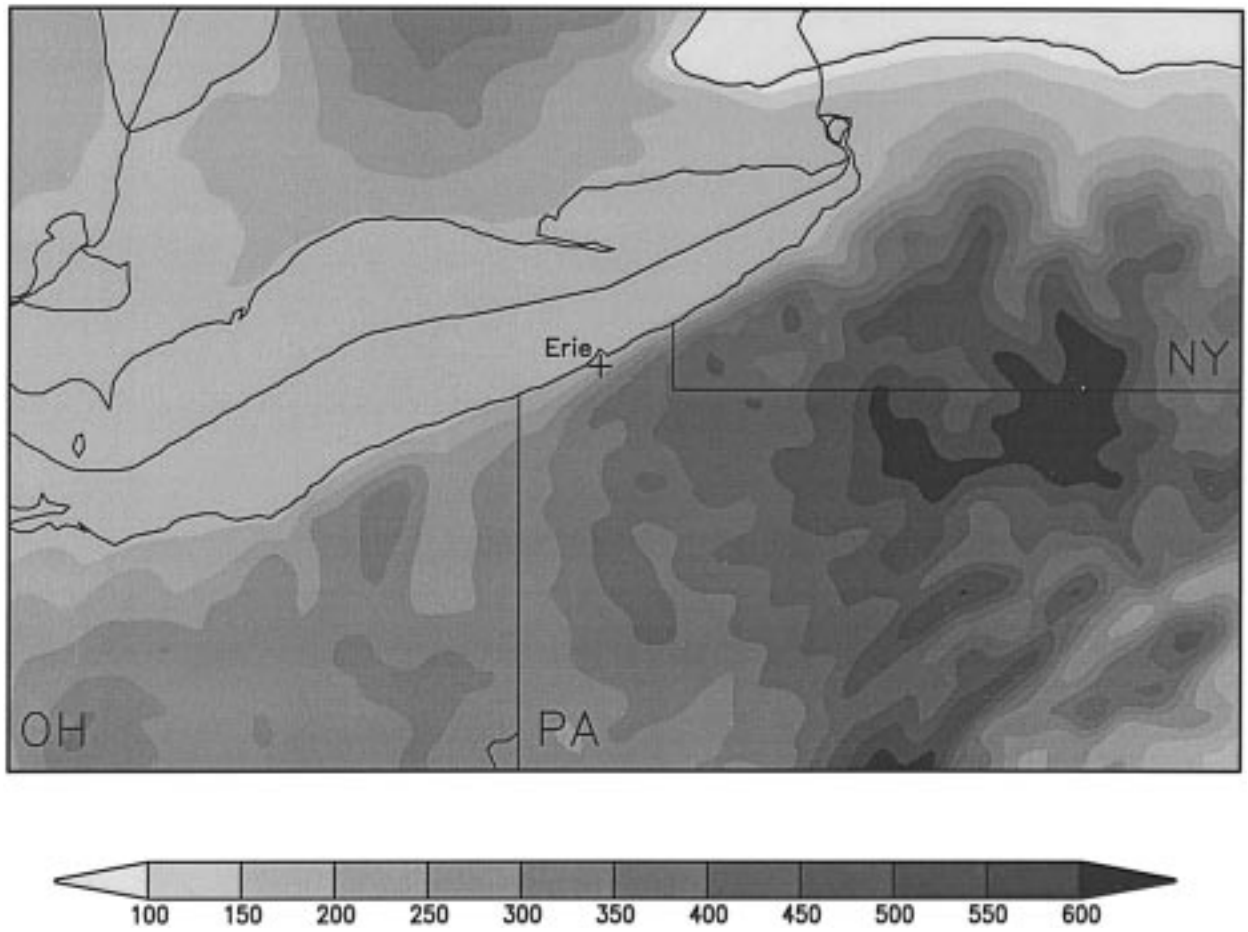

FIG. 15. Terrain map of the Erie, PA, region. Shading interval every 50 m.

vergent flow was directed upslope in northern Erie County, which also likely led to enhancement of the rainband (Fig. 15).

c. Heavy rain production associated with the rainband

The narrow mesoscale rainband that remained nearly stationary just south of the city of Erie was a very efficient rain-producing system. At the height of the event, between 1600 and 1800/17, rainfall rates of 64 mm in 45 min were recorded. A striking characteristic of time-lapse radar imagery was the rapid movement of the precipitation echoes within the band toward the southwest while the larger mass of precipitation echoes (Fig. 6) was moving toward the east and northeast. This implies that the processes forming the precipitation in the rainband were originating primarily in the northeasterly flow of the low levels while the precipitation in the other areas originated at higher levels where the flow was predominantly westerly and southwesterly. Since westerly flow was predominate above 700 hPa, which also was close to the freezing level, it is plausible that the microphysical processes of the large mass of convection on either side of the rainband contained more ice processes than the rainband. In addition, cloud bases to the south and east of the rainband were significantly higher than for the rainband limiting the depth of the above freezing cloud layer. This further suggests that ice processes were important with the larger-scale convection in northwest Pennsylvania.

With a moisture-rich environment in the low levels resulting from air parcels traversing both Lake Ontario and Lake Erie, reported cloud bases in the rainband were very low ($<$150 m). Weckwerth et al. (1996) showed that cloud bases within convective rolls tend to be lower than surrounding clouds due to increases in low-level moisture. Moreover, in a lake-effect snow study, Byrd et al. (1991) showed that an intense single snowband over the lake was characterized by increased low-level moisture and lower cloud bases. With a freezing level close to 700 hPa, the precipitation process in the Erie rainband was likely a warm-rain process over a 3-km-deep layer characterized by collision and coalescence of raindrops. It is also likely that the convection itself, through vertical moisture and heat transport, increased

the depth of the warm-rain processes by lifting the freezing level in the band similar to the results of Byrd et al. (1991). The anomalous depth of the easterly flow within the band (Fig. 13d) suggests, through thermal wind arguments, that the freezing level may have been much higher than 3 km. Furthermore, the WSR-88D data (Figs. 6b, 12, and 13a,b) did not reveal any signs of bright banding in the vicinity of the Erie shoreline rainband, supporting the idea that warm-rain processes were dominate in the rainband.

In addition to the low cloud bases in the Erie region, the air was also locally warmer than surrounding regions. Based upon surface observations, air ascending moist adiabatically from the vicinity of the Erie rainband would have followed a moist adiabat 2–3 K warmer than air only about 25–50 km inland to the southeast over Crawford County, Pennsylvania, where radar data depicted deep convective overturning. In order to examine the effect of the differences in cloud-base height and moist adiabats on the rainfall at the two locations, the one-dimensional cloud model of Anthes (1977) was run for horizontal cloud radii ranging from 1 to 8 km on soundings constructed (as described in section 2) to be representative of the conditions in Erie and Crawford Counties in Pennsylvania. Diagnosed rainfall rates for Erie County were approximately four to five times heavier than that for Crawford County (the average rate for Erie County was 1.7 cm^{-1} vs 0.4 cm h^{-1} for Crawford County).

Operationally, the Cleveland WSR-88D radar underestimated the rainfall amounts within the Erie rainband and overestimated the rainfall in Crawford County and southern Erie County (cf. Figs. 1b and 16a). Thus, the precipitation estimates suggested that heavier precipitation was occurring to the *south* of the rainband over southern Erie and Crawford Counties. Since the Cleveland radar sampled the rainband near Erie at the 3-km (~700 hPa) level, it apparently overshot much of the precipitation that formed from the warm-rain processes below 3 km (Fig. 13c, gray stippling). This situation is similar to the Big Thompson flash flood (Caracena et al. 1979) wherein the convective storm also developed a low echo centroid dominated by warm-rain processes. In that case, the warm cloud layer was about 4 km deep, extending from 3 to 7 km. As in the present case, the nearest radar largely overshot this layer and underestimated the precipitation.

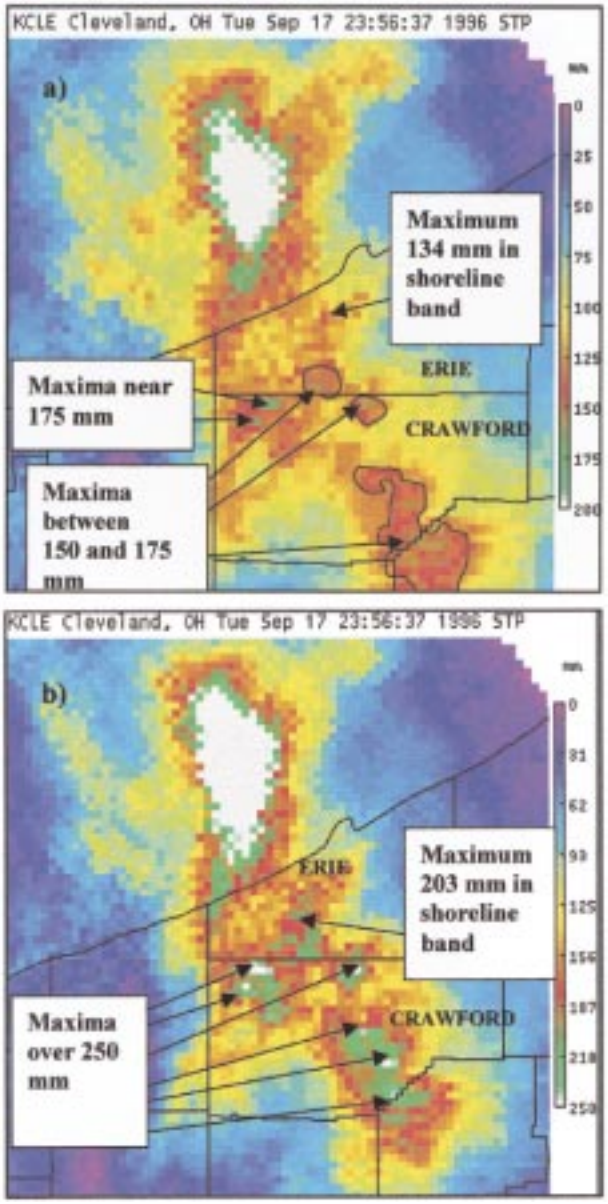

FIG. 16. Cleveland WSR-88D storm-total precipitation 17 Sep 1996 for (a) "normal" NWS Z–R relationship ($Z = 300 \times R^{1.4}$) and (b) "tropical" Z–R relationship ($Z = 250 \times R^{1.2}$).

d. Decay of the rainband and mesoscale precipitation system

Two main factors contributed to the end of the rainfall over Erie county: 1) passage of the short-wave trough and 2) reversal of the regional temperature anomaly such that the warmest air now lay over land instead of over the lake. Similar to Hoxit et al. (1978), Maddox et al. (1977), and Dennis et al. (1973), the heavy rainfall diminished after an upper-level short-wave trough passed by to the east. The passing of the short wave was accompanied by the emergence of strongly divergent low-level radial winds (not shown) as observed by the Cleveland WSR-88D. This signature indicates a transition to subsidence as the short-wave trough passed by.

In addition to the subsidence behind the short wave, a weakening in the temperature gradient over the lake by early afternoon also worked against the continued development of convective rainfall over northwestern Pennsylvania (Fig. 10b). Due to diurnal heating over the land relative to the water, the warm temperature anomaly over Lake Erie in the morning shifted to over

land (except in the area of clouds and precipitation) by early afternoon. With the flow across Lake Erie taking on a more northerly component by midday, slightly cooler and more stable air was flowing into the rainband. The change to a stronger and more northerly low-level wind well inland also may have supported the demise of the mesoscale rainband by dislodging it from Lake Erie as well as weakening the lake-induced convergence zone. The increase in stability, coupled with the subsidence being imposed by the passage of the short wave, and change in the large-scale low-level winds evidently played a role in shutting down the heavy precipitation in Erie, Pennsylvania.

6. Summary and concluding remarks

On 17 September 1996, over 177 mm (7 in.) of rain fell on the southwest side of the city of Erie, Pennsylvania, in a 5-h period. The heavy rain and resulting flash flood were the result of a complex interplay of several scales of forcing, ranging from synoptic to microphysical. The feature most directly responsible for the flood was a quasi-stationary mesoscale rainband. This band was enhanced by a deep unidirectional flow, a strong lake–land temperature gradient, and strong low-level convergence induced by the relatively warm waters of Lake Erie. The band was embedded within a larger-scale area of convection forced by an approaching short wave. The development of the larger-scale convection coincided with two factors that worked to reduce moist static stability in the Erie region: 1) midlevel cooling by adiabatic lifting and horizontal advection associated with the traveling short wave, and 2) warming and moistening of low levels as a result of heat and moisture fluxes from Lakes Ontario and Erie.

When the short-wave forcing arrived, the band deepened and intensified. In addition, as the short wave propagated through the region, the direction of the larger-scale flow rotated in a way that allowed the rainband to push *inland and pivot counterclockwise over the southwestern portion of the city. As a consequence, the heavy rainfall associated with the band persisted in the pivot zone and resulted in the damaging floods.* The counterclockwise rotation of the rainband was accompanied by stronger onshore flow north of the band, which also may have contributed to its intensification. With a more northerly onshore flow on the north side of the band, frictional convergence was maximized and terrain lifting increased. Low-level warm-rain processes were likely active in the rainband for the following reasons: 1) the freezing level was at least 3 km above the surface, 2) cloud bases were around 150 m, and 3) a low-echo centroid was present. The presence of a low-level warm-rain process severely hampered detection of much of the rainfall by the surrounding WSR-88D sites since the radar beam *overshot* most of the lower portion of the cloud.

This case illustrates the difficult nature of estimating precipitation amount by radar owing to the different microphysical processes between the mesoscale rainband and the broader region of convection to the south and east in Erie and Crawford Counties. With active warm-rain processes and a low echo centroid in the rainband, the WSR-88D using the ''normal'' NWS *Z–R* relationship *underestimated* the maximum rainfall near the city of Erie (cf. Figs. 1b and 16a) by up to 40%. The radar simply overshot the higher reflectivities found in the lower portion of the clouds typical of a warm-rain process. In contrast, the precipitation estimates for the larger mass of convection to the south and east of the rainband were *overestimated.* This presents a significant problem to the radar meteorologist since the heavy precipitation of the rainband is ''masked'' by the seemingly heavier precipitation to the south and east. This is especially true if rain gauge and spotter reports are first received from locations to the south of the rainband, which would, therefore, take away credence from the radar precipitation estimates.

Operationally, when an environment conducive to low cloud bases and warm-rain processes is anticipated, the WSR-88D precipitation algorithms can be changed to a ''tropical'' *Z–R* relationship, which accounts for larger rainfall rates with lower reflectivities. This *Z–R* relationship is an attempt to correct for overshooting of the highest reflectivities, which commonly occur with warm-rain processes and low cloud bases. For example, Fig. 16b reveals that the tropical *Z–R* relationship provided a better estimate of rainfall associated with the flood-producing rainband in Erie County. However, Fig. 16b also shows that the tropical *Z–R* overestimated rainfall with the larger area of convection south and east of the rainband by approximately 200%–400%. Thus, again, a forecaster might be led to believe that either the precipitation estimates are significantly overdone or erroneously believe that a *much more widespread* flood event is taking place. This demonstrates that WSR-88D precipitation accumulation algorithms, which are commonly used to estimate precipitation operationally, *can fail over one location and work well over others at the same time.* This event also exemplifies the importance of real-time rainfall gauge data and spotter reports to the NWS flood and flash flood warning programs. It is apparent from this study that short-term prediction and radar detection of the flood were both exceedingly difficult given the present state of the operational forecast models and radar coverage.

Finally, we note that forecasters should be cognizant of early season lake-effect rain events, especially if a short wave is expected to interact with lake-effect rainbands. Forecasters also need to be aware of the problem with detecting heavy rainfall with radar during efficient warm-rain processes associated with low-echo centroids since radar overshooting of the highest reflectivity cores becomes more problematic at longer ranges. In addition, more research is necessary to determine the best strategies for using *Z–R* relationships with the WSR-88D in

conjunction with real-time rainfall gauge data and spotter reports.

Acknowledgments. This paper was produced as part of the requirements for a graduate level class (Mesoscale Analysis 514) in the Department of Meteorology at The Pennsylvania State University. Publication was supported by the National Weather Service. We would like to thank Gary Carter, National Weather Service, Eastern Region Scientific Services division chief, for his initial review of the paper. We would like to acknowledge the anonymous AMS reviewers for improving and clarifying this manuscript. We would also like to thank Richard H. Grumm of the National Weather Service Office in State College for providing the radar and model data for this study and his insightful comments, and David A. Solano, of the Middle Atlantic River Forecast Center in State College, for his assistance in preparing the precipitation figures. We are especially grateful to Dr. Thomas McClain and other National Weather Service weather spotters who provided precipitation rates and totals for Erie County.

APPENDIX

Calculation of Critical Angle for Frictional Convergence

The purpose of this analysis is to relate the pattern of frictionally induced boundary layer convergence that occurred near the Lake Erie shoreline to the synoptic-scale pressure field. In so doing, we aim to explain the amplification of the rainband that occurred between 1500 and 1600 UTC. According to Fig. 14, the band at this time made an angle of about 30° with the Lake Erie shoreline. Because of the deep vigorous convection and the associated tropospheric latent heating, there is undoubtedly a significant contribution to the surface convergence that is not frictionally driven. We demonstrate a close link between band orientation and frictional convergence. While not discarding other explanations for the sudden band amplification, our frictional explanation is certainly plausible.

An approximate way to account for turbulent-viscous forces on airflow near the lower boundary is a simple linear drag characterized by a coefficient, k, proportional to surface roughness and boundary layer stability. Assume that at the shoreline there is a rapid change in k due to roughness being larger, in general, over land than over water. Horizontal convergence or divergence can result from changes in wind speed as well as direction across the shoreline.

Consider the setup in Fig. A1, where a given pressure gradient force of magnitude P exists near the shoreline. Assuming a steady state for that part of the total boundary layer flow linked directly to surface friction, the equations of motion in the x and y directions are, respectively,

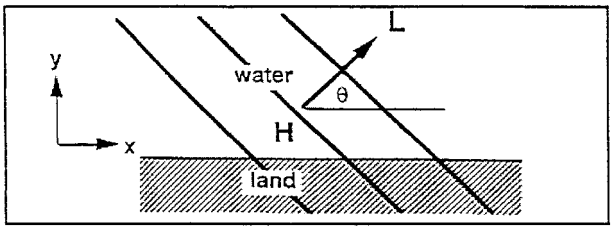

FIG. A1. East–west shoreline and pressure field with orientation angle θ. Arrow shows the pressure gradient force.

$$-ku + fv + P_x = 0, \tag{A1}$$

and

$$-kv - fu + P_y = 0, \tag{A2}$$

P_x and P_y are, respectively, the pressure gradient forces in the x and y directions. Assume that near the east–west-oriented shoreline k decreases with y. There are no variations in the x direction of any parameters in (A1) and (A2). Thus, any divergence or convergence is caused by variations of v, the y component of velocity, with respect to y. Solve (A1) and (A2) for v:

$$v = \frac{kP_y - fP_x}{f^2 + k^2}. \tag{A3}$$

Take the derivative of (A3) with respect to y setting $P_x = P\cos(\theta)$ and $P_y = P\sin(\theta)$, where θ is shown in Fig. A1:

$$\frac{dv}{dy} = \frac{(f^2 - k^2)\sin(\theta) + 2kf\cos(\theta)}{(f^2 + k^2)^2} P\frac{dk}{dy}. \tag{A4}$$

For $0 < \theta < \pi$ low pressure lies to the north of the shoreline; for $0 < \theta < 2\pi$, high pressure lies to the north.

Define a cross-isobar angle, α, of the surface wind with respect to the isobars such that

$$\frac{k}{f} = \tan(\alpha). \tag{A5}$$

Substituting (A5) for k into (A4), the divergence near the shoreline is

$$\frac{dv}{dy} = \frac{[1 - \tan^2(\alpha)]\sin(\theta) + 2\tan(\alpha)\cos(\theta)}{[1 + \tan^2(\alpha)]^2} \frac{P}{f^2}\frac{dk}{dy}. \tag{A6}$$

For a given α and dk/dy, the sign of dv/dy depends on the numerator on the right side of (A6) and thus on the orientation of the isobars with respect to the shoreline.

Figure A2 depicts the dimensionless divergence

$$\left|\frac{dv}{dy}\right|^* \equiv \frac{\dfrac{dv}{dy}}{\dfrac{P}{f^2}\dfrac{dk}{dy}}, \tag{A7}$$

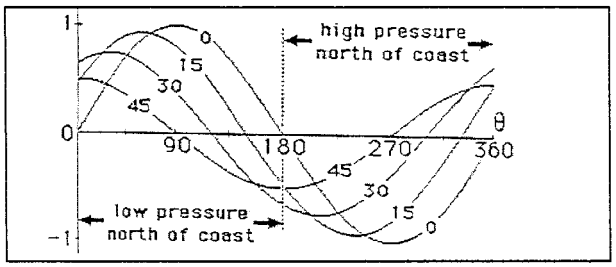

FIG. A2. Dimensionless dk/dy defined in (7) as a function of orientation of the pressure field (θ) for a selection of cross-isobar flow angles (α).

as a function of α and θ. For $\alpha = 30°$ (a typical value), divergence occurs with the isobars parallel to the shoreline and high pressure to the north. Recall that $dk/dy < 0$.

As the low over Maryland at 1200 UTC in Fig. 8a drifted eastward while the high over Canada sat in place, the synoptic-scale pressure field near Erie rotated counterclockwise such that θ increased from approximately 290° at 1200 UTC to 320° by 0000 UTC in Fig. 8e. Let the isobars rotate so that θ increases beyond 270° keeping $\alpha = 30°$ in Fig. A2. Convergence sets in for θ larger than about 305° as the decrease in wind speed over land dominates the divergence due to the changing cross-isobar angle. Thus, according to this simple model, frictionally driven convergence replaces divergence once the surface synoptic-scale isobars achieved an orientation of approximately 35° with respect to the Erie shoreline.

REFERENCES

Anthes, R. A., 1977: A cumulus parameterization scheme utilizing a one-dimensional cloud model. *Mon. Wea. Rev.,* **105,** 270–286.

Ballentine, R. J., G. P. Byrd, and T. A. Niziol, 1993: An operational forecast model for lake-effect snowstorms. Preprints, *13th Conf. on Weather Analysis and Forecasting,* Vienna, VA, Amer. Meteor. Soc., 154–157.

Barnes, S. L., 1964: A technique for maximizing detail in numerical weather map analysis. *J. Appl. Meteor.,* **3,** 396–409.

Black, T. L., 1994: The new NMC mesoscale ETA model: Description and forecast examples. *Wea. Forecasting,* **9,** 265–278.

——, D. G. Deaven, and G. DiMego, 1993: The step-mountain ETA coordinate model: 80 km ''Early'' version and objective verifications. Technical Procedures Bull. 412, NOAA/NWS, 31 pp. [Available from National Weather Service, Office of Meteorology, 1325 East–West Highway, Silver Spring, MD 20910.]

Byrd, G. P., R. A. Anstett, J. E. Heim, and D. M. Usinski, 1991: Mobile sounding observations of lake-effect snowbands in western and central New York. *Mon. Wea. Rev.,* **119,** 2323–2332.

Cahir, J. J., J. M. Norman, and D. A. Lowry, 1981: Use of a real time computer graphics system in analysis and forecasting. *Mon. Wea. Rev.,* **109,** 485–500.

Caracena, F., R. A. Maddox, L. R. Hoxit, and C. F. Chappell, 1979: Mesoanalysis of the Big Thompson storm. *Mon. Wea. Rev.,* **107,** 1–17.

Dennis, A. S., R. A. Schleusener, J. H. Hirsch, and A. Koscielski, 1973: Meteorology of the Black Hills flood of 1972. Institute of Atmospheric Sciences Rep. No. 73-4, South Dakota School of Mines and Technology, 41 pp. [Available from Institute of Atmospheric Sciences, South Dakota School of Mines and Technology, Rapid City, SD 57701.]

Fritsch, J. M., and R. L. Vislocky, 1996: Enhanced depiction of surface weather features. *Bull. Amer. Meteor. Soc.,* **77,** 491–506.

Hill, J. D., 1971: Snow squalls in the lee of Lakes Erie and Ontario. NOAA Tech. Memo. NWS ER-43, 20 pp. [NTIS COM-72-00959.]

Hjelmfelt, M., 1990: Numerical study of the influence of environmental conditions on lake-effect snowstorms on Lake Michigan. *Mon. Wea. Rev.,* **118,** 138–150.

Holroyd, E. W., III, 1971: Lake-effect cloud bands as seen from satellites. *J. Atmos. Sci.,* **28,** 1165–1170.

Hoxit, L. R., and Coauthors, 1978: Meteorological analysis of the Johnstown, Pennsylvania flash flood, 19–20 July 1977. NOAA Tech. Rep. ERL 401-APCL 43, 71 pp. [NTIS PB-297412.]

Jiusto, J. E., 1971: Crystal development and glaciation of a super cooled cloud. *J. Rech. Atmos.,* **5,** 69–85.

Lavoie, R. L., 1972: A mesoscale numerical model of lake-effect storms. *J. Atmos. Sci.,* **29,** 1025–1040.

Lenschow, D. H., 1973: Two examples of planetary boundary layer modification over the Great Lakes. *J. Atmos. Sci.,* **30,** 568–581.

Maddox, R. A., 1980: An objective technique for separating macroscale and mesoscale features in meteorological data. *Mon. Wea. Rev.,* **108,** 1108–1121.

——, F. Caracena, L. R. Hoxit, and C. F. Chappell, 1977: Meteorological aspects of the Big Thompson flash flood of 31 July 1976. NOAA Tech. Rep. ERL 388-APCL 41, 83 pp. [NTIS PB-275191.]

Miner, T., and J. M. Fritsch, 1997: Lake-effect rain events. *Mon. Wea. Rev.,* **125,** 3231–3248.

Niziol, T. A., 1987: Operational forecasting of lake-effect snowfall in western and central New York. *Wea. Forecasting,* **2,** 310–321.

Petterssen, S., and P. A. Calabrese, 1959: On some weather influences due to warming of the air by the Great Lakes in winter. *J. Meteor.,* **16,** 646–652.

Sousounis, P. J., and J. M. Fritsch, 1994: Lake-aggregate mesoscale disturbances. Part II: A case study of the effects on regional and synoptic-scale weather systems. *Bull. Amer. Meteor. Soc.,* **75,** 1793–1811.

Weckwerth, T. M., J. W. Wilson, and R. M. Wakimoto, 1996: Thermodynamic variability within the convective boundary layer due to horizontal convective rolls. *Mon. Wea. Rev.,* **124,** 769–784.

Young, G., and J. M. Fritsch, 1989: A proposal for general conventions in analysis of mesoscale boundaries. *Bull. Amer. Meteor. Soc.,* **70,** 1412–1421.